Absorption of one-dimensional dielectric–metal photonic-crystal absorbers for terahertz range

Tarek I Alanazi

Department of Physics, College of Science, Northern Border University,
Arar 73222, Saudi Arabia, tarek.alanazi@nbu.edu.sa

Received: 06.01.2023

Abstract. We study the spectral response of a one-dimensional dielectric–metal photonic-crystal absorber. The reflection and absorption spectra in the frequency range 0.1–10 THz are obtained by applying a transfer-matrix method. The influence of different factors such as the incidence angle, the thickness and the materials of metallic and dielectric layers on the absorption spectrum of our absorber is explored. Finally, we offer a high-efficient photonic-crystal absorber based on Si–Ni with the free spectral range 1.46 THz and the finesse 2.496. The calculations reveal that high enough absorption (99.37%) and reflection (96.77%) can be achieved for our absorber. Therefore, it can be used as both a perfect absorber and a perfect reflector over a wide range of THz frequencies.

Keywords: optical absorption, one-dimensional photonic crystals, transfer-matrix method, terahertz absorbers, dielectric–metal stacks

UDC: 535.3

1. Introduction

Optical absorbers are devices that can absorb electromagnetic waves. They have gained a great research interest in the recent years because of their various applications, including photodetectors [1, 2], spectroscopy [3, 4] and photovoltaic systems [5, 6]. Broad- and narrow-band absorbers can be classified according to their absorption bandwidths. A narrow-band absorber can be used for sensing purposes [7] and filtering applications [8, 9]. In contrast, wide-band absorbers are primarily used in radar cross-section reduction [10], stealth technologies [11] and solar-based devices [12, 13]. The absorbers are employed in different frequency ranges such as ultraviolet, visible, infrared and terahertz (THz) ones [14–17]. Even though terahertz absorbers have received a little attention, the terahertz range itself has prominent advantages like a high resolution, a deep penetrability and low energy consumption [18–20].

The optical absorbers have been reported in different schemes, e.g. in photonic crystals (PhCs), metamaterial structures and metal–insulator–metal configurations. The PhCs represent artificial structures with periodically changing refractive index. These refractive-index changes can be made along a single dimension, two dimensions or three dimensions, which results in one-dimensional (1D), two-dimensional (2D) or three-dimensional (3D) PhCs, respectively. The refractive index and the thickness of each layer in a PhC determine the performance of appropriate absorber. In the PhCs made of dispersive materials, the performance depends on the incident wavelength because the refractive indices vary sharply. Therefore, the spectral response of this absorber must be thoroughly considered. The simplest type of the PhC is 1D, which is created by alternating layers with different refractive indices. The appropriate fabrication process is straightforward and usually uses a chemical vapour-deposition method [21]. Up to date, the PhCs have been used in various optical devices like waveguides

[22], filters [23], modulators [24], logic gates [25] and absorbers [26]. The 1D PhCs can be all-dielectric or represent stacks of metal–dielectric layers. In general, only a portion of the incident light is transmitted through the all-dielectric structures, while the remainder is reflected or absorbed.

On the contrary, a minimal amount of the incident light is transmitted through the structures composed of metal and dielectric stacks, and a high percentage of it is reflected and/or absorbed. In general, metals prevent the propagation of electromagnetic waves and totally reflect the incident light. It is possible to increase the absorption of the 1D PhCs using thin metal layers. It is also possible to design such structures in order to increase the reflection or the transmission, depending on the thickness and the permittivity of the layers and the operating frequency [27]. Since the permittivity difference between dielectrics and metals is large, a fewer periods are required to obtain the desired optical properties [28].

Various optical PhC-based absorbers have been developed in the recent years. Most of them are based on the all-dielectric PhC structures. For example, an absorber that operates on an all-dielectric PhC structure and a metallic substrate and utilizes s so-called optical Tamm state has been reported by Lu et al. [29]. The device manifests the absorption 90% in the visible range. The transmission characteristics of a PhC made of Ag metal and GaN dielectric have been studied by Choi et al. [30]. Chen et al. [31] have studied experimentally the spectral response of a 1D Ag–SiO_2 PhC inside the wavelength region 200–800 nm. They have shown that increasing number of periods can increase the total absorption of the structure.

With the advent of graphene, several works have been devoted to the design of 1D PhC absorbers for the THz range. So, Li et al. have suggested a THz graphene-based PhC for filtering applications [32]. Here a 1D PhC filter consists of sequential stacks of graphene layers alternated with dielectric layers, with two defect dielectric layers in the middle of the structure. It works at the frequencies from 5.5 THz to 7.5 THz. In the other work, Fan et al. have reported a broadband THz absorber based on a 1D graphene-embedded PhC structure [33]. The maximum average absorption of the absorber is 28.8% for the frequency range 0.1–10 THz. Unfortunately, little attention has been paid to the dielectric–metal PhC absorbers that operate in the THz range. In the present work, we study the spectral response of the dielectric–metal PhC absorbers in the range 0.1–10 THz and their effective absorption parameters.

2. Structure of the absorber and its theory

A scheme of the 1D PhC structure is represented in Fig. 1. It consists of subsequent layers of a dielectric D and a metal M, with the corresponding permittivities ε_d and ε_m. The thicknesses of the dielectric and metal layers are given respectively by d_d and d_m, thus resulting in the periodicity with the period $a = d_d + d_m$ and the total number N of the periods. In our calculations, the permittivities of the input (ε_0) and output (ε_{N+1}) planes correspond to the air. Furthermore, all the materials are supposed to be nonmagnetic ($\mu_r = 1$). The layers are arranged inside the xy plane and the electromagnetic field with the wave vector of k_0 propagates at the angle θ_0 with respect to the z axis.

Different techniques have been employed for solving the Maxwell's equations in the 1D PhC structures. These are a Green-function method [34], a plane-wave expansion method [35, 36], a finite-difference time-domain method [37, 38], a transfer-matrix method [39] and a finite-element method [40]. All-numerical techniques of the finite-difference time domain and finite elements are characterized by a large amount of calculations. They require powerful simulation facilities and are time-consuming. These limitations become more severe when the structure has skinny layers. On the contrary, semi-analytical techniques such as the transfer-matrix method provide accurate enough results in a short time with common simulation facilities.

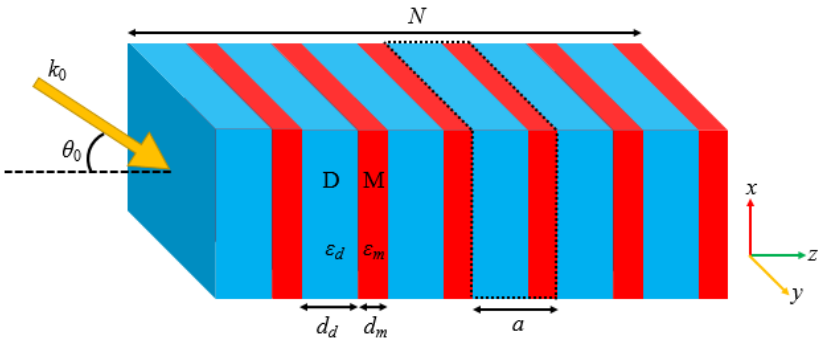

Fig. 1. A 3D view of a 1D dielectric–metal PhC absorber.

Let the width of j^{th} layer is equal to d^t. One can find the following relationship for the tangential components of the electric and magnetic fields at the interfaces [41]:

$$M_j = \begin{bmatrix} \cos\left(\xi_j\right) & \frac{1}{\psi_j}\sin\left(\xi_j\right) \\ \psi_j \sin\left(\xi_j\right) & \cos\left(\xi_j\right) \end{bmatrix}. \tag{1}$$

Here ξ_j amounts to $k_0 d_j \sqrt{n_j^2 - \sin^2\theta_0}$. Then one can obtain $\psi_j = 1/\sqrt{n_j^2 - \sin^2\theta_0}$ and $\psi_j = n_j^2/\sqrt{n_j^2 - \sin^2\theta_0}$ respectively for the TE and TM polarizations, with n_j indicating the refractive index of the jth layer. The same approach can also be applied to the metallic layer. Considering the complex refractive index $N_j = n_j + i\kappa_j$ (with κ_j being the imaginary part), one can express the propagation angle for the j^{th} layer [41] by the relation

$$\cos\left(\theta_j\right) = \left(\sqrt{N_j^2 - \sin^2\theta_0}\right)/N_j. \tag{2}$$

By multiplying the matrices of all the subsequent layers, we arrive at the total transfer matrix:

$$M = (M_d M_m)^N = \begin{bmatrix} m_{11} & m_{12} \\ m_{21} & m_{22} \end{bmatrix}. \tag{3}$$

Since the PhC is surrounded by air, the refractive indices of the first (n_0) and last (n_{N+1}) layers are unit. The complex coefficients of transmission and reflection can be derived from the transfer matrix as follows [41]:

$$t(\lambda) = \frac{2\cos\theta_0}{\left(m_{11} + m_{22}\right)\cos\theta_0 + i\left(m_{12}\cos^2\theta_0 - m_{21}\right)}, \tag{4}$$

$$r(\lambda) = \frac{(m_{11} + m_{22})\cos\theta_0 - i(m_{12}\cos^2\theta_0 - m_{21})}{(m_{11} + m_{22})\cos\theta_0 + i(m_{12}\cos^2\theta_0 - m_{21})}. \tag{5}$$

Here λ is the light wavelength. The reflection (R) and transmission (T) parameters can be obtained from the relations $R(\lambda) = |r(\lambda)|^2$ and $T(\lambda) = |t(\lambda)|^2$, respectively. Therefore, the absorption A is given by the formula $A(\lambda) = 1 - T(\lambda) - R(\lambda)$.

3. Numerical results and discussion

Let the dielectric is assumed to be silica, SiO_2. Its permittivity can be taken from the work by D. Palik [42]. The permittivity for Ag can be calculated using a known Drude–Lorentz model. We

have taken the number of the poles and the values of the constants in the model from the work [43]. The initial thicknesses of the dielectric and metal layers are $d_d = 30$ μm and $d_m = 5$ nm, respectively, thus giving the period $a = 30.005$ μm. Let the number of periods be equal to $N = 10$. Fig. 2 shows the reflection, transmission and absorption spectra of the absorber at the normal incidence for the frequencies from 0.1 to 10 THz. The oscillating behaviour is due to the Fabry–Perot resonances occurring among the metallic and dielectric layers. While the incident wave travels through the structure, only a few wavelengths resonate, i.e. they are reflected back and forth by the two metals at each period, until all the input power is reflected or absorbed.

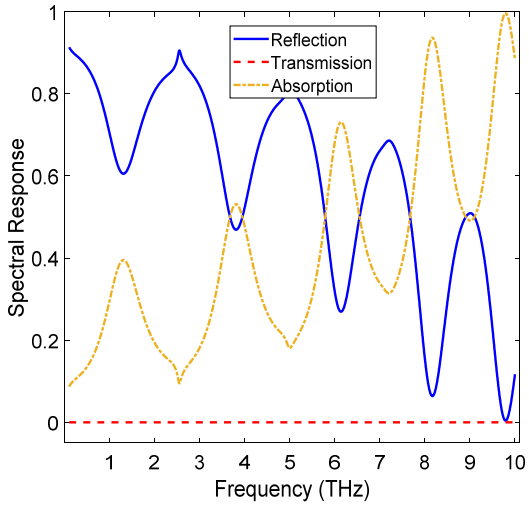

Fig. 2. Spectral response of our 1D PhC absorber: $D = SiO_2$, $M = Ag$, $d_d = 30$ μm and $d_m = 5$ nm.

We accept that the transmission is zero ($T \sim 10^{-6}$ in the frequency range under study), which is attributed to the metal layers. As the frequency increases, the reflection of the structure decreases while the absorption increases. Let us consider the parameter $A_{avg} = \int_{f_{min}}^{f_{max}} A(f)df / (f_{max} - f_{min})$ as the average absorption, where $A(f)$ is the frequency-dependent absorption spectrum, and f_{max} and f_{min} indicate the limits of the desired frequency range. Then the average absorption 41.54% can be obtained at the normal incidence for the case of $f_{min} = 0.1$ THz and $f_{max} = 10$ THz.

Since the structure is symmetric along the x and y directions, the absorber behaves identically for both the TE (i.e., the S-wave) and TM (the P-wave) polarizations. When the incident angle becomes nonzero, the spectral responses of the absorber for TM and TE polarization change. To study this effect, we calculate the reflection and absorption spectra for the TE and TM polarizations in the range 0°–85° of the incident angles. Fig. 3a and Fig. 3b display respectively the reflection and absorption spectra for the TE polarization as functions of the frequency and the incident angle. It is obvious that the structure reflects most of the incident light at the frequencies lower than 8 THz.

The absorption is a dominant phenomenon at higher frequencies. For the incident light with the TM polarization, the absorption at higher frequencies is larger than that of the TE polarization. For example, more than 80% of the incident light is absorbed at the frequencies from 9.6 to 10 THz, independently from the incident angle. Therefore, the structure acts as a perfect angle-insensitive absorber in this range. Fig. 4 shows the average absorption for each incident angle in the frequency range 0.1–10 THz. The highest absorption is 47.25%, which is achieved for the TM polarization and the incident angle $\theta = 67°$.

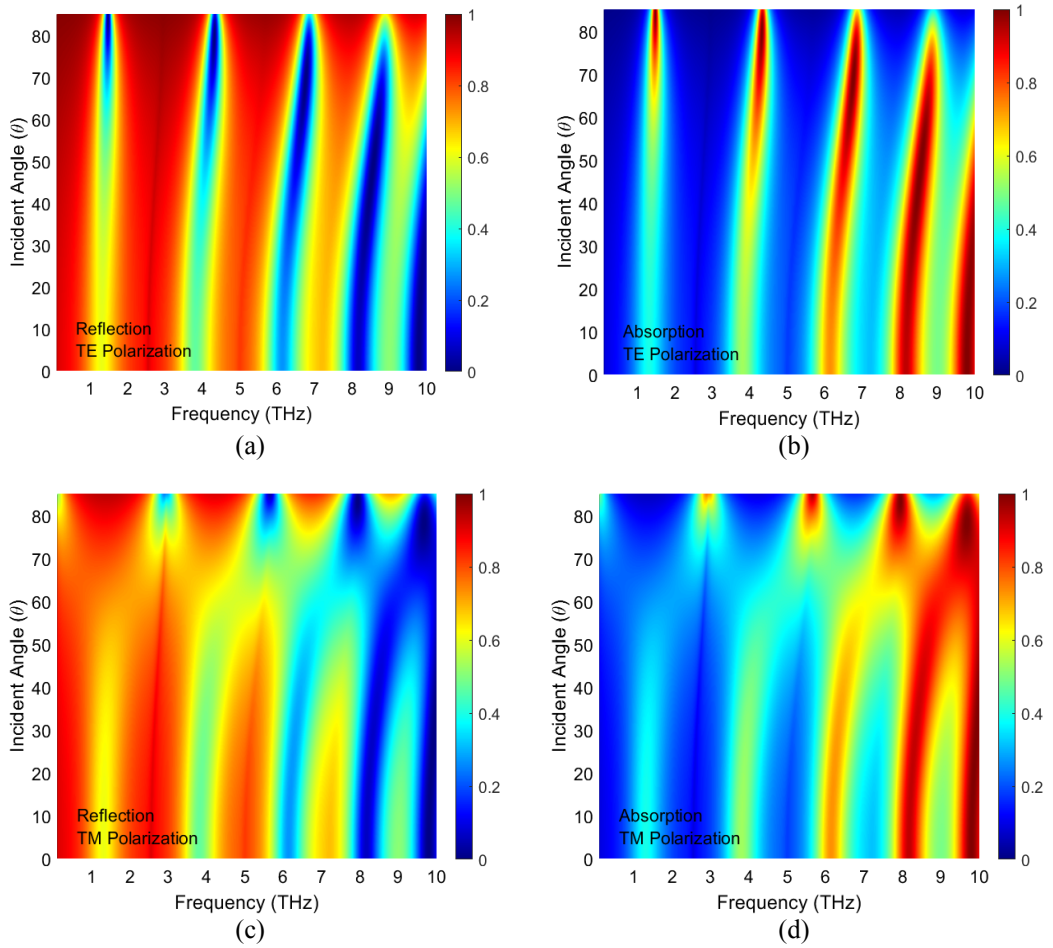

Fig. 3. Reflection (a) and absorption (b) spectra for the TE polarization, and reflection (c) and absorption (d) spectra for the TM polarization, as calculated for our 1D PhC absorber at different incident angles.

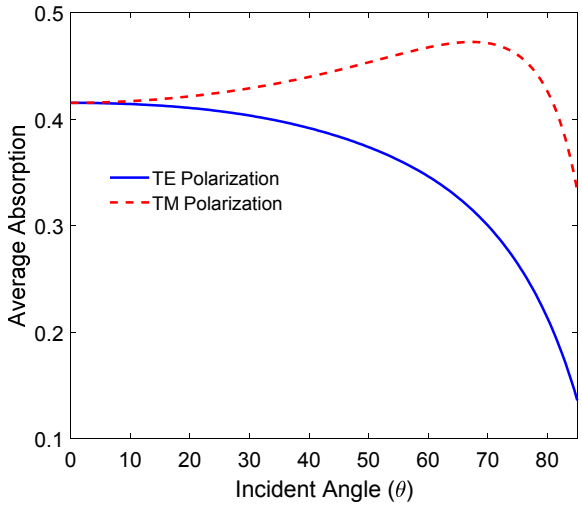

Fig. 4. Average absorption A_{avg} of our 1D PhC absorber as a function of incident angle for the TE and TM polarizations.

The performance of the 1D PhC absorber depends on both the thicknesses and the materials of the layers. To have a deeper insight into this matter, in the following subsection we study the effects of these two factors on the absorber's performance.

3.1. Thicknesses of the layers

As the 1D PhC suggested by us is composed of the two types of materials, dielectric and metal, we should change the thicknesses of these layers and determine the reflection and absorption spectra of the absorber. In the dielectric–metal PhCs, thin metal layers should be used; otherwise, the incident wave is totally reflected. Therefore, we first set the thicknesses of the metal layers to be d_m = 5 nm and change the thicknesses d_d of the dielectric layers from 0.2 to 100 μm. As seen from Fig. 5, larger thicknesses of the dielectric layers result in higher absorption for the normal incidence of radiation. The absorption of our absorber increases with increasing thicknesses of the dielectric layers. Furthermore, the absorption increases at higher frequencies at a fixed d_d value, so that over 70% of the incident light with the frequencies higher than 8 THz is absorbed at the dielectric thicknesses larger than 55 μm.

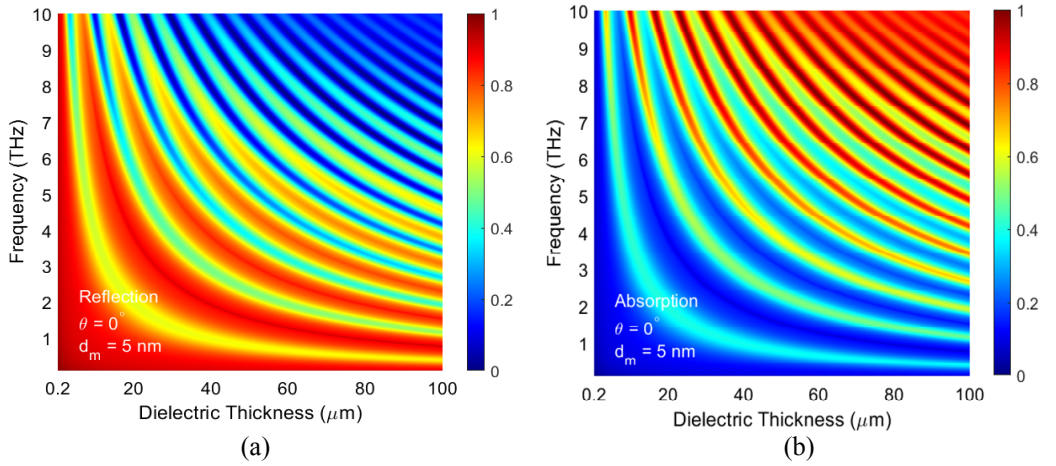

Fig. 5. Reflection (a) and absorption (b) spectra of our 1D PhC absorber versus the dielectric thickness d_d: D = SiO_2, M = Ag, d_m = 5 nm and θ = 0°.

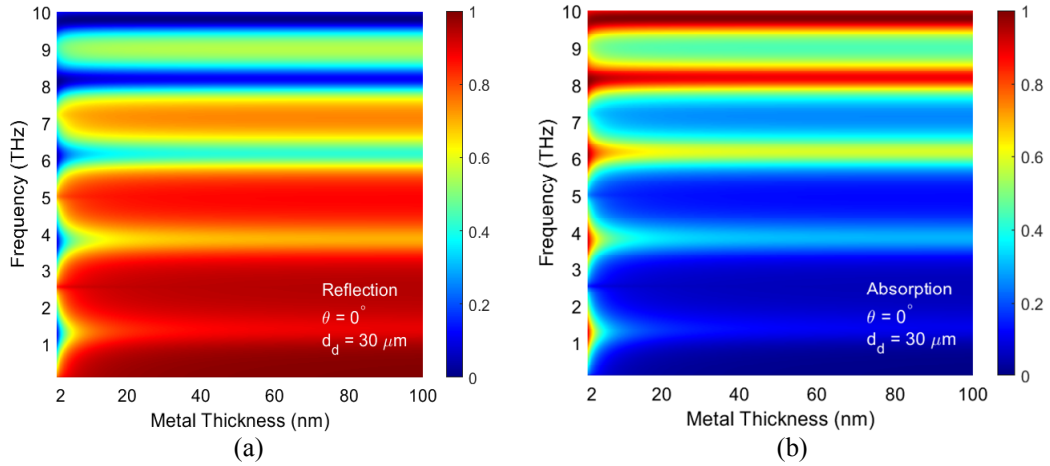

Fig. 6. Reflection (a) and absorption (b) spectra of our 1D PhC absorber versus the metal thickness d_m: D = SiO_2, M = Ag, d_d = 30 μm and θ = 0°.

Now we scrutinize the effect of the thicknesses of the metal layers. To this end, the thicknesses of the dielectric layers are set to be d_d = 30 μm and the thicknesses of the metal layers are altered from 2 to 100 nm. Fig. 6a and Fig. 6b illustrate respectively the reflection and

absorption spectra of our absorber. At the d_m values larger than 10 nm, the absorber operates independently of the thicknesses of the metal layer. It is known that the permittivity of metals depends on the frequency. As a result, the metals reveal different optical properties for the electromagnetic waves with different frequencies. As the frequency increases, the metal layers' reflection is reduced and more of the incident light is absorbed. For the waves with the frequencies higher than 7.7 THz, more than half of the incident radiation is absorbed, regardless of the thickness of the metal layer.

3.2. Materials of the layers

Now we investigate the effect of metal and dielectric materials on the performance of our structure. The geometrical parameters are fixed at d_d = 30 μm and d_m = 5 nm. First, we change the material of the metal layers. The absorption spectra of the absorber are analyzed for such metals as gold (Au), aluminium (Al), nickel (Ni) and tungsten (W), while the material of the dielectric layer is SiO_2. The permittivities of Al, Au, Al, Ni and W can be calculated using the Drude–Lorentz model. The corresponding constants for each metal are taken from the work [43]. The real and imaginary parts of the permittivity of these metals are plotted on a logarithmic scale in Fig. 7. Ni and W metals have similar real and imaginary parts of the permittivity. Moreover, it is seen form Fig. 7 that Ni and W have a higher real part Re(ε) of the permittivity than the other metals.

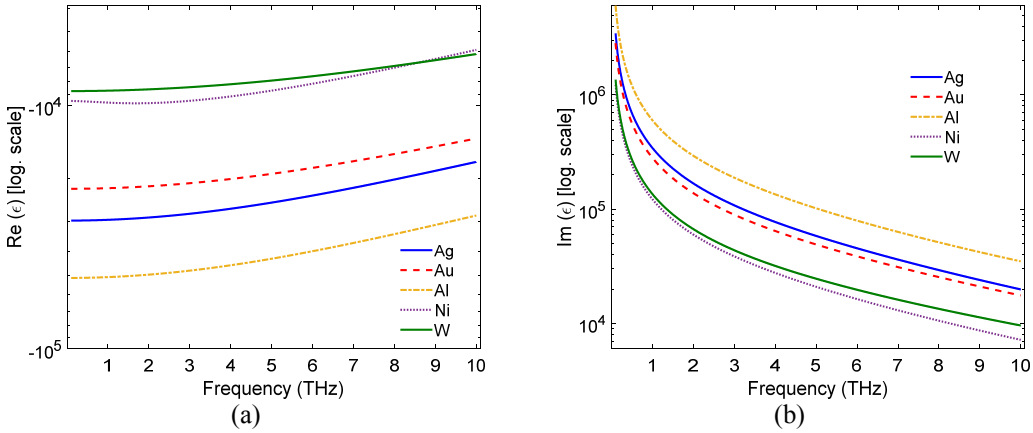

Fig. 7. Real (a) and imaginary (b) parts of permittivity shown for the Ag, Au, Al, Ni and W metals on a logarithmic scale in the frequency range 0.1–10 THz.

On the other hand, Ni and W have the lowest imaginary part Im(ε) of the permittivity. So it can be predicted that the PhCs with Ni–SiO_2 and W–SiO_2 materials should have similar absorption spectra. Fig. 8a shows the absorption spectra of the corresponding absorbers. The absorber with the Ni layers reveals the highest absorption. Under the condition of normal incidence, the average absorption values obtained for the absorbers with the Au, Al, Ni and W layers and the SiO_2 dielectric layers are equal to 43.81, 36.71, 56.37 and 54.53%, respectively.

The same studies have been performed for the case of different dielectric layers. Here the metal layers correspond to Ag and the material of the dielectric layers is changed to alumina (Al_2O_3) and silicon (Si). The refractive indices of Al_2O_3 and Si have also been taken from Ref. [42]. The absorption spectra derived for the absorbers with the SiO_2, Al_2O_3 and Si dielectric layers are shown in Fig. 8b. The absorbers with Si and Al_2O_3 layers have higher absorption peaks at lower frequencies. The average absorptions 34.81 and 27.98% are achieved for the absorbers with Al_2O_3 and Si. Note that the Si-based absorber reveals a periodic behaviour. The peaks and

dips in the absorption spectrum for the Si–Ag absorber are constant regardless of frequency, thus leading to a fixed free spectral range (FSR). This brings to mind the idea that an absorber with a high absorption and a periodic behaviour in the frequency range under test can be implemented by changing the materials of the PhC.

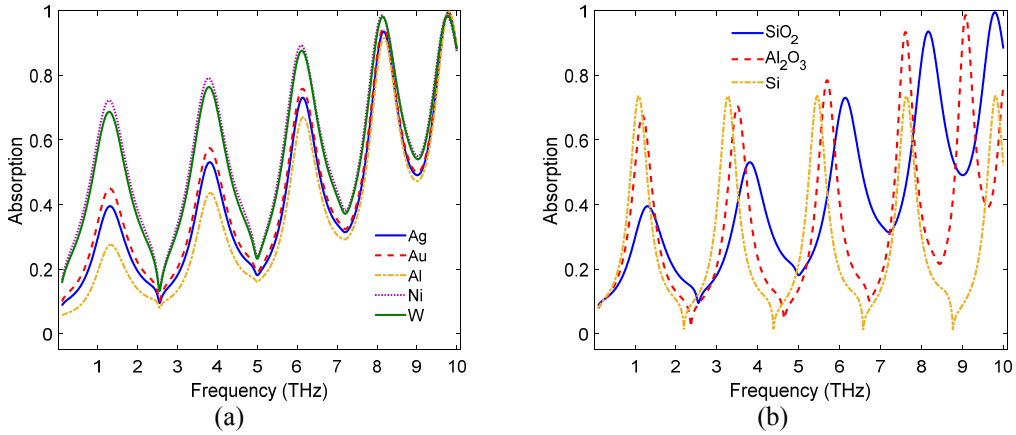

Fig. 8. Absorption spectra of our 1D PhC absorber for different metals and SiO_2 dielectric layers (a) and different dielectrics and Ag metal layers (b).

Fig. 9 displays the absorption spectra of the absorber, which involves the metallic Ni layers and the dielectric Si layers, as functions of the incidence angle for the TE and TM polarizations. This absorber offers a constant FSR, 1.46 THz. The finesse parameter F defined as F = FSR/FWHM (with FWHM being the full width at half of the maximum) is calculated to be 2.496 for the case of FWHM = 0.585 THz. A great feature of this absorber is that it can be operated independently from the incidence angle and exhibits a perfect absorption in the absorption bands for the incident angles up to 75°. The average absorption of this absorber is 48.99% for the normal incidence. Furthermore, the maximal and minimal absorptions are respectively 99.37 and 3.23% for the normal incidence, which makes this device a perfect absorber and reflector.

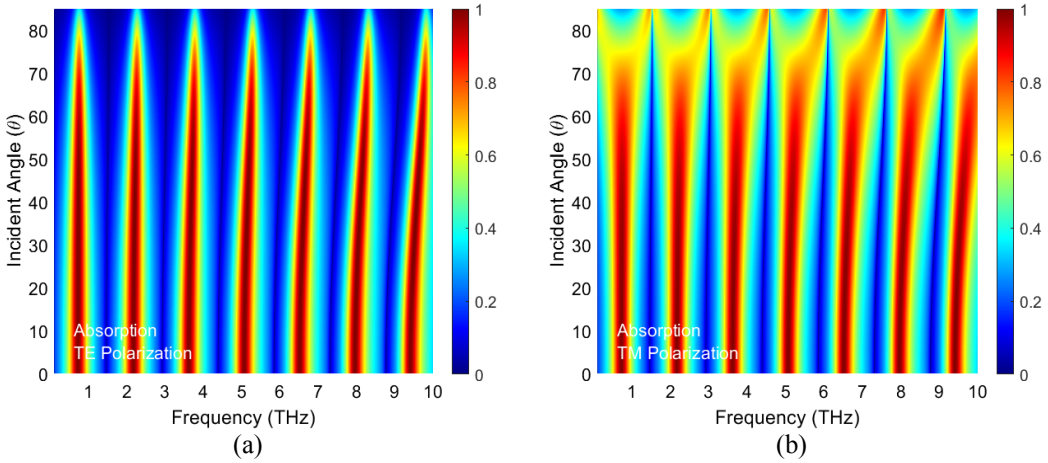

Fig. 9. Absorption spectra of our 1D PhC absorber with Ni metallic layers and Si dielectric layers versus the incident angle for TE (a) and TM (b) polarizations.

In spite of a simple structure and common materials, the absorbers suggested by us have a great performance in the THz range. Note that, as already mentioned, graphene is also used to

design the 1D PhC absorbers operating in the THz range [32, 44]. Graphene represents a mono-layer of carbon with the thickness 0.34 nm. The main characteristic of the graphene-based structures is their adjustability achieved due to application of external voltage. Due to a very low thickness of graphene, a significant amount of the incident light is transmitted, which results in a relatively low total absorption of the structure. Moreover, fabrication of such absorbers is a kind of challenge. Therefore, the 1D PhC structures based upon some more common materials like those utilized in this work represent a suitable choice for many absorbing, sensing and filtering applications.

4. Conclusion

We have discussed the spectral response of the 1D PhC absorber based on sequential dielectric and metallic layers. The results obtained by the transfer-matrix method reveal a goof performance of the SiO_2–Ag PhC absorber for the TM polarization under oblique irradiation. We show that increasing thickness of the dielectric layers results in higher absorption values. However, the thickness of the metal layers has a negligible effect at the thicknesses larger than 10 nm. Changes in the PhC materials change the absorption-spectrum patterns, which provides an adjustable average absorption varying from 27.98 to 56.37%. The Si–Ni PhC absorber reveals the constant FSR 1.46 THz and the finesse 2.496 in the wide frequency range 0.1–10 THz. The maximal and minimal absorption values achieved for this absorber are equal to 99.37 and 3.23%, respectively.

Acknowledgment. The author is grateful to the Prince Faisal bin Khalid bin Sultan Research Chair in Renewable Energy Studies and Applications (PFCRE) at Northern Border University for their support and assistance.

Conflict of interest. The author declares that there is no conflict of interest regarding the publication of this manuscript.

References

1. Zhu Y, Yu P, Ashalley E, Liu T, Lin F, Ji H, Takahara J, Govorov A and Wang Z, 2020. Planar hot-electron photodetector utilizing high refractive index MoS_2 in Fabry–Pérot perfect absorber. Nanotechn. **31**: 274001.
2. Chen Z, Weng Y, Liu J, Guo N, Yu Y and Xiao L, 2021. Dual-band perfect absorber for a mid-infrared photodetector based on a dielectric metal metasurface. Photon. Res. **9**: 27–33.
3. Korkmaz S, Turkmen M and Aksu S, 2020. Mid-infrared narrow band plasmonic perfect absorber for vibrational spectroscopy. Sens.Actuat. A: Phys. **301**: 111757.
4. Bailey M L P, Pierce A T, Simon A J, Edwards D T, Ramian G J, Agladze N I, Sherwin M S, 2015. Narrow-band water-based absorber with high return loss for terahertz spectroscopy. IEEE Trans. Terahertz Sci. Technol. **5**: 961–966.
5. Li X, Zhong X, Hu Y, Li B, Sheng Y, Zhang Y, Weng C, Feng M, Han H and Wang J, 2017. Organic–inorganic copper (II)-based material: A low-toxic, highly stable light absorber for photovoltaic application. J. Phys. Chem. Lett. **8**: 1804–1809.
6. Wu C, Neuner B III, John J, Milder A, Zollars B, Savoy S, Shvets G, 2012. Metamaterial-based integrated plasmonic absorber/emitter for solar thermo-photovoltaic systems. J. Opt. **14**: 024005.
7. Luo S, Zhao J, Zuo D and Wang X, 2016. Perfect narrow band absorber for sensing applications. Opt. Express. **24**: 9288–9294.
8. Tan J, Wu Z, Xu K, Meng Y, Jin G, Wang L, Wang Y, 2020. Numerical study of an Au–ZnO–Al perfect absorber for a color filter with a high quality factor. Plasmonics. **15**: 293–299.

9. Yu Y, Qian Q, Wang C, Fan L, Cheng L, Chen H, Zhao L, 2022. An all-dielectric metasurface long-pass cut-off filter based on a multi-nanocircular array perfect cut-off absorber. Microwave Opt. Technol. Lett. **64**: 300–304.
10. Sun H, Gu C, Chen X, Li Z, Liu L, Xu B, Zhou Z, 2017. Broadband and broad-angle polarization-independent metasurface for radar cross section reduction. Sci. Rep. **7**: 1–9.
11. Chakradhary V K, Baskey H B, Roshan R, Pathik A and Akhtar M J, 2018. Design of frequency selective surface-based hybrid nanocomposite absorber for stealth applications. *I*EEE Trans. Microwave Theory and Techniques. **66**: 4737–4744.
12. Mehrabi S, Rezaei M H and Rastegari M R, 2021. High-efficient plasmonic solar absorber and thermal emitter from ultraviolet to near-infrared region. Opt. Laser Technol. **143**: 107323.
13. Langlais M, Bru H and Ben-Abdallah P, 2014. High temperature layered absorber for thermo-solar systems. J. Quant. Spectr. Rad. Trans. **149**: 8–15.
14. Charola S, Patel S K, Dalsaniya K, Jadeja R, Nguyen T K and Dhasarathan V, 2021. Numerical investigation of wideband L-shaped metasurface based solar absorber for visible and ultraviolet region. Physica B: Condens. Matter. **601**: 412503.
15. Xu R and Takahara J, 2021. Radiative loss control of an embedded silicon perfect absorber in the visible region. Opt. Lett. **46**: 805–808.
16. Pitchappa P, Ho C P, Kropelnicki P, Singh N, Kwong D-L and Lee C, 2014. Dual band complementary metamaterial absorber in near infrared region. J. Appl. Phys. **115**: 193109.
17. Fu P, Liu F, Ren G J, Su F, Li D and Yao J Q, 2018. A broadband metamaterial absorber based on multi-layer graphene in the terahertz region. Opt. Commun. **417**: 62–66.
18. Wang M and Yang E-H, 2018. THz applications of 2D materials: graphene and beyond. Nano-Struct. Nano-Obj. **15**: 107–113.
19. Tonouchi M, 2007. Cutting-edge terahertz technology. Nature Photon. **1**: 97–105.
20. Borak A, 2005. Toward bridging the terahertz gap with silicon-based lasers. Science. **308**: 638–639.
21. Shen H, Wang Z, Wu Y and Yang B, 2016. One-dimensional photonic crystals: fabrication, responsiveness and emerging applications in 3D construction. RSC Adv. **6**: 4505–4520.
22. Withayachumnankul W, Fujita M and Nagatsuma T, 2018. Integrated silicon photonic crystals toward terahertz communications. Adv. Opt. Mat. **6**: 1800401.
23. Hosseinzadeh Sani M, Ghanbari A and Saghaei H, 2020. An ultra-narrowband all-optical filter based on the resonant cavities in rod-based photonic crystal microstructure. Opt. Quant. Electron. **52**: 1–15.
24. Li M, Ling J, He Y, Javid U A, Xue S and Lin Q, 2020. Lithium niobate photonic-crystal electro-optic modulator. Nature Commun. **11**: 1–8.
25. Safinezhad A, Babaei Ghoushji H, Shiri M and Rezaei M H, 2021. High-performance and ultrafast configurable all-optical photonic crystal logic gates based on interference effects. Opt. Quant. Electron. **53**: 1–20.
26. Wang X, Liang Y, Wu L, Guo J, Dai X and Xiang Y, 2018. Multi-channel perfect absorber based on a one-dimensional topological photonic crystal heterostructure with graphene. Opt. Lett. **43**: 4256–4259.
27. Wang Z, Chan C T, Zhang W, Ming N and Sheng P, 2001. Three-dimensional self-assembly of metal nanoparticles: Possible photonic crystal with a complete gap below the plasma frequency. Phys. Rev. B. **64**: 113108.
28. Sigalas M.M, Chan C T, Ho K and Soukoulis C M, 1995. Metallic photonic band-gap materials. Phys. Rev. B. **52**: 11744.

29. Lu G, Zhang K, Zhao Y, Zhang L, Shang Z, Zhou H, Diao C and Zhou X, 2021. Perfect optical absorbers by all-dielectric photonic crystal/metal heterostructures due to optical Tamm state. Nanomater. **11**: 3447.
30. Choi Y-K, Ha Y-K, Kim J-E, Park H Y and Kim K, 2004. Antireflection film in one-dimensional metallo-dielectric photonic crystals. Opt. Commun. **230**: 239–243.
31. Chen S, Wang Y, Yao D and Song Z, 2009. Absorption enhancement in 1D Ag/SiO_2 metallic–dielectric photonic crystals. Opt. Appl. **39**: 473–479.
32. Li Y, Qi L, Yu J, Chen Z, Yao Y and Liu X, 2017. One-dimensional multiband terahertz graphene photonic crystal filters. Opt. Mater. Express. **7**: 1228–1239.
33. Fan Y, Tu L, Zhang F, Fu Q, Zhang Z, Wei Z, Li H, 2018. Broadband terahertz absorption in graphene-embedded photonic crystals. Plasmonics. **13**: 1153–1158.
34. D'Aguanno G, Mattiucci N, Scalora M, Bloemer M and Zheltikov A, 2004. Density of modes and tunneling times in finite one-dimensional photonic crystals: a comprehensive analysis. Phys. Rev. E. **70**: 016612.
35. Segovia-Chaves F and Vinck-Posada H, 2018. Temperature dependence of defect mode in band structures of the one-dimensional photonic crystal. Optik. **154**: 467–472.
36. Jiang B, Zhou W-J, Chen W, Liu A-J and Zheng W-H, 2011. Improved plane-wave expansion method for band structure calculation of metal photonic crystal. Chin. Phys.Lett. **28**: 034209.
37. Pratibha K, Sinngh M, Soni S, Garg T, Tuli V, Gaurav S, Shankar S, 2022. Influence of defect layer of ZnS/air on one dimensional photonic crystal structure of gallium phosphide-crown glass using lumerical FDTD. J. Optoel. Adv. Mater. **24**: 230–235.
38. Çetin A, 2020. Transmission properties of defect modes with different defect layer geometries in one-dimensional photonic crystals. Int. J. Engin. Sci. Inv. (IJESI). **9**: 56-60.
39. Zaky Z A, Sharma A, Alamri S and Aly A H, 2021. Theoretical evaluation of the refractive index sensing capability using the coupling of Tamm–Fano resonance in one-dimensional photonic crystals. Appl. Nanosci. **11**: 2261–2270.
40. Elmahdy N A, Esmail M S and Mohamed M, 2018. Characterization of a thermal sensor based on one-dimensional photonic crystal with central liquid crystal defect. Optik. **170**: 444–451.
41. Jamshidi-Ghaleh K and Ebrahimpour Z, 2013. One-way absorption behaviour in defective 1D dielectric–metal photonic crystal. Europop. Phys. J. D. **67**: 1–4.
42. Palik E D. Handbook of optical constants of solids. Vol. 3. Elsevier Inc., 1997.
43. Rakić A D, Djurišić A B, Elazar J M and Majewski M L, 1998. Optical properties of metallic films for vertical-cavity optoelectronic devices. Appl. Opt. **37**: 5271–5283.
44. Tavana S, Zarifkar A and Miri M, 2022. Tunable terahertz perfect absorber and polarizer based on one-dimensional anisotropic graphene photonic crystal. IEEE Photon. J. **14**(3): 1–9.

Tarek I Alanazi 2023. Absorption of one-dimensional dielectric–metal photonic-crystal absorbers for terahertz range. Ukr.J.Phys.Opt. **24**: 83 – 94. doi: 10.3116/16091833/24/1/83/2023

Анотація. *Досліджено спектральний відгук одновимірного діелектрично-металевого фотонно-кристалічного поглинача. Спектри відбиття та поглинання в діапазоні частот 0,1–10 ТГц одержано за методом матриці перенесення. Досліджено вплив різних факторів, таких як кут падіння випромінювання, товщина та матеріали металевих і діелектричних шарів, на спектр поглинання поглинача. Запропоновано високоефективний фотонно-кристалічний поглинач на основі Si–Ni з вільним спектральним діапазоном 1,46 ТГц і F-фактором різкості 2,496. Розрахунки показали, що з нашим поглиначем можна досягти і*

високого поглинання (99,37%), і високого відбивання (96,77%). Тому його можна використовувати як ідеальний поглинач та ідеальний відбивач у широкому діапазоні терагерцових частот.

***Ключові слова**: поглинання, одновимірні фотонні кристали, метод матриці переносу, терагерцові поглиначі, діелектрично-металеві стопи*